PROCEEDINGS, 41st Workshop on Geothermal Reservoir Engineering
Stanford University, Stanford, California, February 22-24, 2016
SGP-TR-209

Geomechanical Analysis of EGS Reservoir Development in Normal, Strike-Slip and Thrust Faulting Terrains

Aleta Finnila[1], William Dershowitz[1], and Robert McLaren[2]

[1]Golder Associates Inc., 18300 Union Hill Road, Redmond WA 98052 USA

[2]Golder Associates Ltd., 210 Sheldon Dr., Cambridge, Ontario, N1T1A8 Canada

afinnila@golder.com

Keywords: enhanced geothermal systems (EGS), discrete fracture network (DFN), block size analysis, hydraulic fracturing, hydro-shearing

ABSTRACT

Stimulation by hydro-shearing and hydraulic fracturing changes the intensity of significant conducting fractures and their transmissivities in EGS reservoirs. These changes lead to a variety of preferential flow path geometries which affect the thermal and impedance performance of the reservoir. Starting with geologically realistic discrete fracture network (DFN) models in differing regional stress states, this paper examines the evolution of block size measures during lower pressure, longer duration hydro-shearing stimulation and the resulting stimulated fractures apertures and transmissivities. Block size and shape are shown to significantly influence reservoir thermal depletion. As stimulation pumping-pressure increases, the significant fractures for thermal production align with the minimum stress direction while flow is preferentially channeled in the maximum horizontal stress direction. In normal and strike-slip stress regions, fractures may open preferentially at shallower depths due to larger differentials between the pumping pressure and the in situ stresses, thus driving flow-path creation towards shallower, cooler rock.

1. INTRODUCTION

Hydraulic stimulation is the most commonly used technique to improve the performance of deep heat reservoirs targeted for EGS projects (Breede et al., 2013). An injection well is drilled and water injected at pumping pressures sufficient to cause shear failure in existing natural fractures, a process referred to as hydro-shearing. If pumping pressure is sufficient to raise the pressure at depth to the minimum principal stress level, then hydraulic fracturing will occur with the formation of induced tensile fractures. This paper explores the evolution of these flow paths combining hydro-sheared natural fractures and induced hydraulic fractures using archetypical DFN models developed in a previous paper representing normal, strike-slip and thrust faulting regions of the United States (Finnila et al., 2015). The models are evaluated at a range of stimulation levels: before stimulation where the pore pressure is hydrostatic (0%), a maximum level of stimulation where pore pressure equals the minimum principal stress and hydraulic fracturing occurs (100%), and three intervals in between (25%, 50%, and 75%). The paper addressed the selection of pumping pressures required to create economically viable flow rates, the production water temperatures to be expected over the lifetime of the EGS project, and how production and injection wells should be configured.

For the purpose of this study, an economically productive geothermal system for the purpose of this paper is defined as one that can sustain water flow rates of 70 l/s with a system impedance less than 0.15 MPa/(l/s) at temperatures above 180°C for a period of at least 20 years (JASON, 2013; Idaho National Laboratory, 2006).

The parameters for the archetypical DFN models studied are provided in Table 1. The in situ stress state varies between the three models corresponding to differing regional tectonic conditions: extensional, strike-slip, and compressional. The rock properties and natural fracture characteristics are typical of known igneous and metamorphic rock formations for the corresponding tectonic conditions. The models share the same reservoir dimensions, thermal gradient, and depth. Injection and production wells are separated by 800 m with a third stimulation well located between in between. Well orientations in the target area are horizontal for the extensional and strike-slip models and vertical for the compressional model. These configurations were selected to maximize intersections with critically stressed and induced fractures. Initial natural fracture transmissivities are in the range 10^{-8} to 10^{-7} m^2/s such that the natural rock mass hydraulic conductivity is insufficient for a conventional geothermal system. The rock matrix is treated as effectively impermeable.

The stimulation for each of the archetypical DFN models was implemented using a 3D geomechanical simulator (Golder Associates, 2015). For each stimulation, the simulator evaluated the induced effective stress state at the well and on connected natural fractures. Induced hydraulic fractures grow in the model where injection pressure exceeds the minimum stress. Natural fractures that reach the Mohr-Coulomb failure criterion in shear are designated as “hydrosheared”. The increase in fracture transmissivity due to hydro-shearing was estimated using multipliers of 10, 100, and 1000 based on the reported values of 24 from Desert Peak, Nevada (Dempsey, 2014) and 1000 from Basel, Switzerland (Miller, 2015).

Coupled heat and mass flow simulations were carried out using both pre-stimulation and stimulated DFN models (Therrien and Sudicky, 1996; Brunner and Simmons, 2012) to determine whether the models can support the required flow-rates, impedance

restrictions, and heat production history. For each model, the rock block size and shape is calculated for comparison to the hydraulic and thermal performance measures.

Reservoir Properties		**General Fracture Properties**	
Reservoir Dimensions	2 km x 2 km x 1 km	Initial Transmissivity	Correlated to Size
Thermal Gradient	60°C/km	Initial Aperture	0.3*Transmissivity^0.3
Well Depth	3.5 km	Initial Storativity	0.0016* Transmissivity ^0.17
Water Properties		Number of Sides	6
Density [kg/m3]	1000		
Thermal Conductivity [W/m°C]	0.68		
Heat Capacity [J/kg°C]	4180		
	Extensional	**Strike-Slip**	**Compressional**
	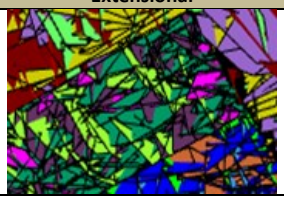	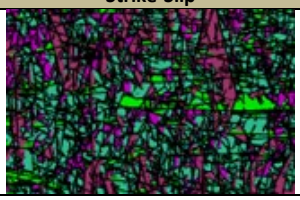	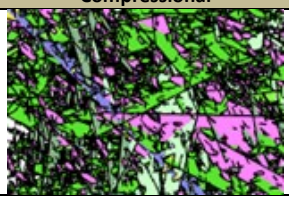
Stress State			
Maximum Stress σ_1 [MPa/km]	Vertical, 90°: 25	Horizontal, 135°: 27	Horizontal, 50°: 30
Intermediate Stress σ_2 [MPa/km]	Horizontal, 25°: 17	Vertical, 90°: 24.1	Horizontal, 140°: 25
Minimum Stress σ_3 [MPa/km]	Horizontal, 115°: 15	Horizontal, 45°: 16	Vertical, 90°: 22.3
Pore Pressure [MPa/km]	Hydrostatic: 9.9	Hydrostatic: 9.9	Hydrostatic: 9.9
Rock Properties			
Rock Type	Metavolcanic	Basalt	Granite
Density ρ [kg/m^3]	2,650	2,800	2,600
Heat Capacity C [J/kg°C]	700	680	750
Thermal Conductivity K [W/m°C]	1.9	2.2	3.0
Young's Modulus E [GPa]	34.2	80	40
Poisson's ratio υ	0.18	0.25	0.25
Fracture Properties			
Set Name; Trend[deg]/Plunge [deg]; Volumetric Fracture Intensity P_{32} [1/m]	Normal; 25°/60°; 0.045 Vertical; 115°/0°; 0.03 Bedding; 295°/30°; 0.015 Random; 0°/0°; 0.005	Horizontal; 135°/90°; 0.03 Vertical 1; 25°/0°; 0.1 Vertical 2; 115°/0°; 0.05	Horizontal; 90°/83°; 0.15 Vertical; 310°/8°; 0.15 Inclined; 285°/40°; 0.15
Fracture pole orientation shown on lower hemisphere, equal angle stereonet	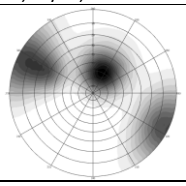	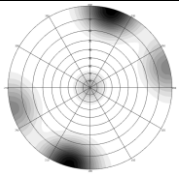	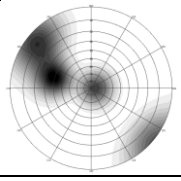
Length/Height Aspect Ratio	3	3	1
Mean Transmissivity T [m^2/s]	1.1×10^{-7}	9.3×10^{-8}	1.9×10^{-8}
Min/Max Radius R [m]	20/500	25/500	10/500
Shear Strength Criterion	Mohr-Coulomb	Mohr-Coulomb	Mohr-Coulomb
Cohesion c [MPa], Friction angle ϕ [deg]	0, 30°	0, 30°	0, 30°
Well Geometry	Horizontal	Horizontal	Vertical
	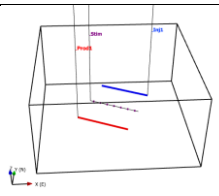	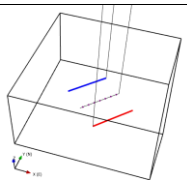	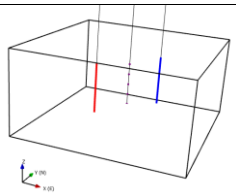

Table 1. Model Parameters (Finnila et al., 2015).

2. HYDRO-SHEARING AND CRITICAL STRESS

As illustrated in Table 2, the orientation of critically stressed fractures from hydro-shearing stimulation is determined by the relationship between the natural fracture sets and the stress state. Critically-stressed fractures are oriented in conjugate sets at (45° +/- ϕ/2) symmetric about the minimum principal stress direction, σ_3. Results provided in Table 2 indicate that the three archetypical models

respond differently to hydraulic stimulation. Both the extensional stress state model and the strike-slip model are close to shear-failure even before stimulation which results in having a significant number of the pre-existing fractures reach critical stress at the lowest modeled stimulation level of 25%. In contrast, the compressional stress model doesn't have any critically stressed fractures until the 75% stimulation level is reached. With its much higher values for the principal stresses, the compressional stress model is very difficult to stimulate, requiring a surface pumping pressure of 32.5 MPa to achieve the 75% stimulation level. Hydraulic fracturing in the compressional stress model occurs at 17.8 MPa surface pumping pressure.

Comparing the location of critically stressed fractures on the stereonets in Table 2 with the natural fracture set orientations shown in Table 1, it is evident that the extensional stress model natural fracture sets do not generally align with the orientation of conjugate shear orientation (45° +/- ϕ/2) at which the first fractures fail in shear, while the natural fractures in the strike-slip stress model do. This results in having 57% of all the fractures in the strike-slip stress model failing in shear at a 25% stimulation level while the extensional stress model only has 22%. The high number of fractures having enhanced transmissivity at the 25% stimulation level is sufficient to provide highly conductive flow paths for the strike-slip stress model and, therefore, no further stimulation was simulated.

Stimulation Level in Range between Hydrostatic Pore Pressure and Hydraulic Fracture Limit			
0%	**25%**	**50%**	**75%**
Extensional			
0 MPa	4.5 MPa	8.9 MPa	13.4 MPa
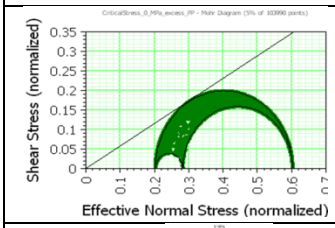	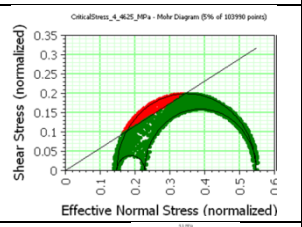	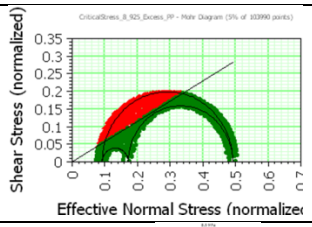	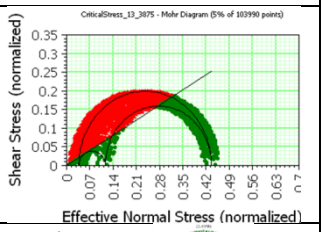
0% 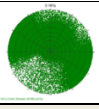	22% 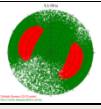	39% 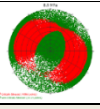	62% 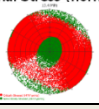
Strike-Slip			
0 MPa	5.3 MPa		
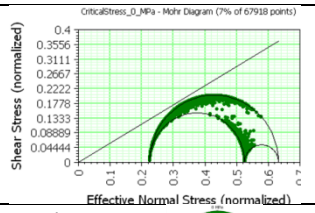	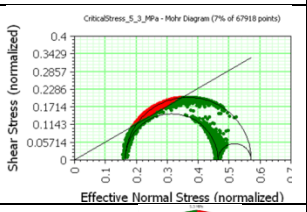		
0% 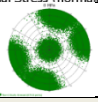	57% 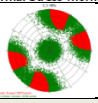		
Compressional			
0 MPa	10.9 MPa	21.7 MPa	32.5 MPa
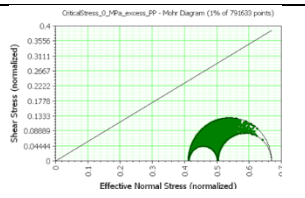	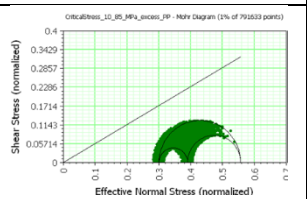	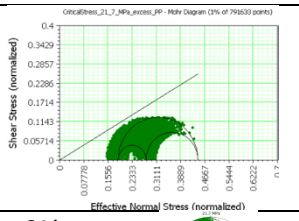	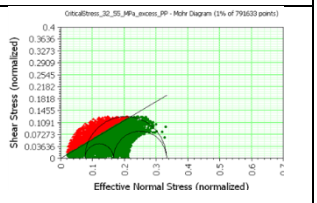
0% 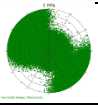	0% 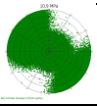	0% 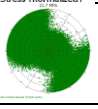	28% 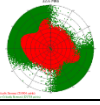

Table 2. Critically stressed fractures [red] at stimulation levels in the range between hydrostatic pore pressure and the minimum principal stress. For each of the three stress state models, the first row shows the excess pore pressure added, the second row shows a Mohr diagram with normal and shear stresses normalized by the maximum stress, and the third row shows the orientation of the fractures in a lower hemisphere, equal angle, polar stereonet. The percentage included in the third row signifies the percent of fractures which are critically stressed.

Once the critically stressed fractures are identified at each stimulation level, the transmissivity of these hydro-sheared natural fractures is assumed to increase by a factor of 10, 100 or 1000. The natural fractures in the three models are well-connected, such that injection pressures are assumed to propagate to all the fractures in the model. For the current study, a compartmentalized flow assumption was made, with no pressure decline with distance into the network. If the center of a fracture is calculated to be critically stressed, than the transmissivity of the entire fracture is increased. This simplification along with not restricting transmissivities to be below a maximum may result in overestimating the conductance of the system, especially at deeper levels. These assumptions will be reconsidered in future studies.

At the 100% stimulation level, induced tensile fractures are generated (Golder Associates, 2015). These fractures form normal to σ_3, the minimum principal stress direction, and are created so as to span the distance between the injection and production wells. The set of fractures present at the 100% stimulation level include these new hydraulic fractures as well as fractures having enhanced transmissivity due to hydro-shearing. Figure 1 shows the hydraulic fractures formed in the extensional stress model and illustrates how these vertical fractures tend to open more at shallower depths. Note that the inflated apertures shown are based on the injected volumes. The hydraulic apertures expected following stimulation will be smaller and will depend on the proppant penetration.

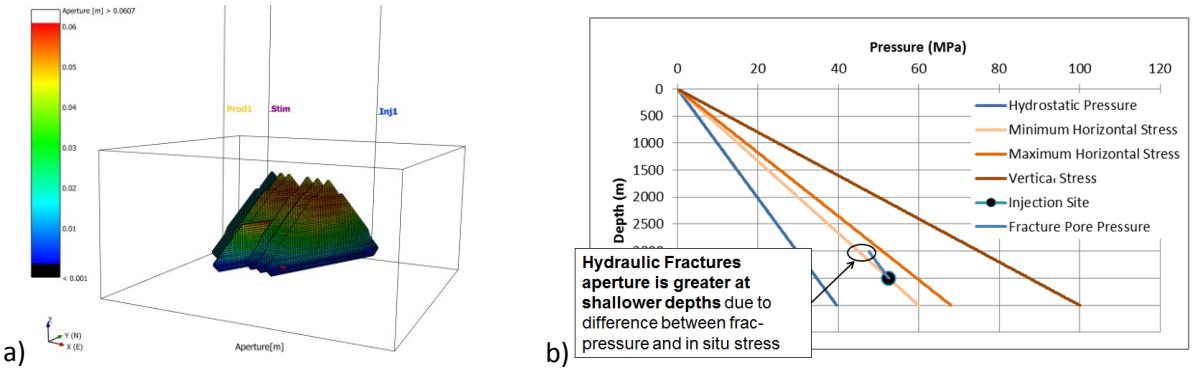

Figure 1. Extensional stress model hydraulic fractures (a), and stress gradients illustrating why vertical fractures drive flow to cooler zones (b).

3. TESTING FLOW RATES AND IMPEDANCE

The results of flow simulations in the DFN models (Miller et al., 2005) are shown in Figure 2. A constant head boundary was assumed at the wells and no-flow boundaries were assumed on the faces of the model. At each stimulation level, the head on the injection well was set to the equivalent stimulation level pressure while the production well was maintained at zero head at the surface. The reported flow rate is therefore the maximum possible for that stimulation level. A range of connected fracture set sizes was used. The largest and most transmissive fractures were included in the sets and the vertical spread shown in Figure 2 between models having the same transmissivity factor at the same percent excess stimulation pore pressure reflects the variance you could expect from flow localization.

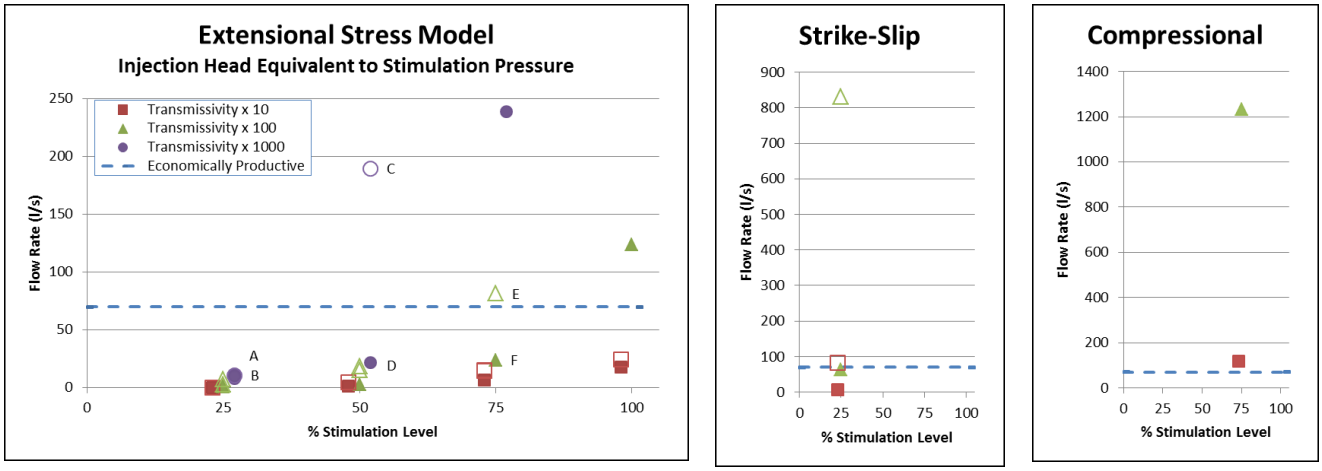

Figure 2. Flow rates vs excess pore pressure percentage between hydrostatic and the hydraulic fracture limit. Open, larger symbols indicate simulation includes more than 1000 fractures. Numbers of fractures modeled ranged from approximately 10 to 8000. Labels A-F refer to simulations included in thermal modeling.

As shown in Figure 2, flow rates of 70 l/s were achieved for the extensional stress model at the 50% stimulation level assuming that critically stressed fracture transmissivities were enhanced by a factor of 1000 and that significant flow localization was not an issue. If

fracture transmissivities are only increased by a factor of 100, then the extensional stress model requires a 75% stimulation level as well as no significant flow localization. If transmissivities are enhanced only by a factor of 10, then no amount of hydro-shearing yields an economic system. This is not the case for the strike-slip or compressional stress models. As you can see on the right side of Figure 2, the strike-slip stress model can achieve flow rates over 70 l/s at the 25% stimulation level even with a transmissivity factor of only 10. The compressional stress model can achieve that flow rate, but not until a stimulation level of 75% is reached.

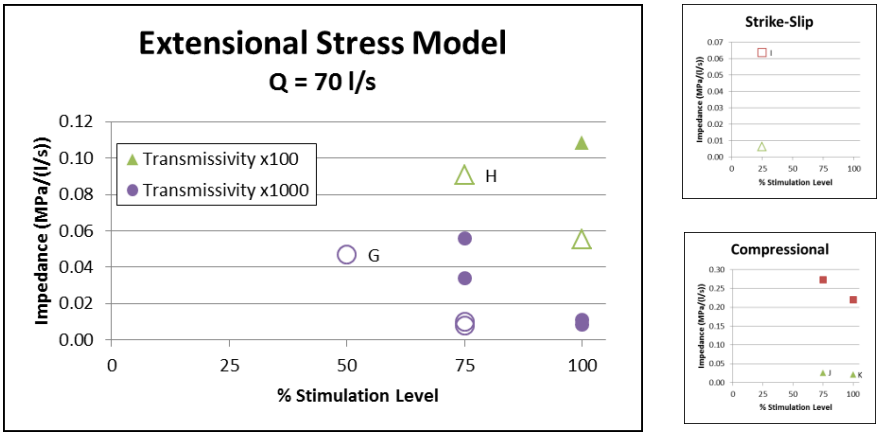

Figure 3. Impedance vs stimulation level using a fixed flow rate of 70 l/s. Open, larger symbols indicate simulation includes more than 1000 fractures. Numbers of fractures modeled ranged from approximately 10 to 4300. Red data points on the Strike-Slip and Compressional charts are for models having critically stressed fracture transmissivities increased by a factor of 10. Labels G-K indicate simulations included in thermal modeling.

Figure 3 shows the impedance between the injection well and a production well for those models that could achieve a flow rate of 70 l/s. These simulations were carried out using constant flux boundary conditions on the wells, with the injection well having a positive flow rate of 70 l/s and the production well having a negative rate of 70 l/s. As expected, impedance values were consistent between simulations having the same fractures and fracture properties regardless of which type of boundary condition was applied.

4. TESTING THERMAL DRAWDOWN

Once a model shows it can sustain economic flow rates, the next test is to determine how the production water temperature will decline during production. Connected sets of the largest and most transmissive fractures in the model were simulated using the same boundary conditions as were used for the flow rate and impedance simulations in a coupled heat and mass flow simulation (Therrien and Sudicky, 1996; Brunner and Simmons, 2012).

Based on the results shown in Figure 2 for the extensional stress model, DFNs were chosen for thermal modeling which showed the nearest match to economic flow rates at each hydro-shearing stimulation level. For stimulation levels of 25% and 50%, the models assumed that critically stressed fracture transmissivity increased by a factor of 1000. The model simulated for the 75% stimulation level assumed transmissivities increased by a factor of 100. Figure 4a shows their flow rates and production water temperature over time. These simulations were carried out under constant head conditions where the injection well head was set to the stimulation level pressure: 25% used a surface head of 455 m, 50% used a surface head of 910 m and 75% used a surface head of 1,365 m and the production well surface head was set to zero. These simulations therefore calculate the maximum flow rate possible through the model for the various stimulation levels.

The effects of flow localization are suggested in Figure 4a by considering simulations with varying conductive fracture intensity. Simulations with greater connected fracture intensity showed increased flow rates and higher production temperatures (solid lines). Restricting the flow to fewer fractures resulted in lower flow rates and more rapid thermal decline (dashed lines). While the production temperatures of the model experiencing 25% stimulation stay high, the flow rates are too low at 11 l/s even with the assumption of a factor of 1000 for transmissivity enhancement (light purple lines). At 50% stimulation, a model using a factor of 1000 transmissivity enhancement can also fail to maintain high temperatures if the flow rates are too high (dark purple solid line) or if flow localization is too prevalent (dark purple dashed line). At a stimulation level of 75%, models having critically stressed fracture transmissivities enhanced by a factor of 100 or more can produce flow rates above 70 l/s, although flow localization can degrade performance (green lines).

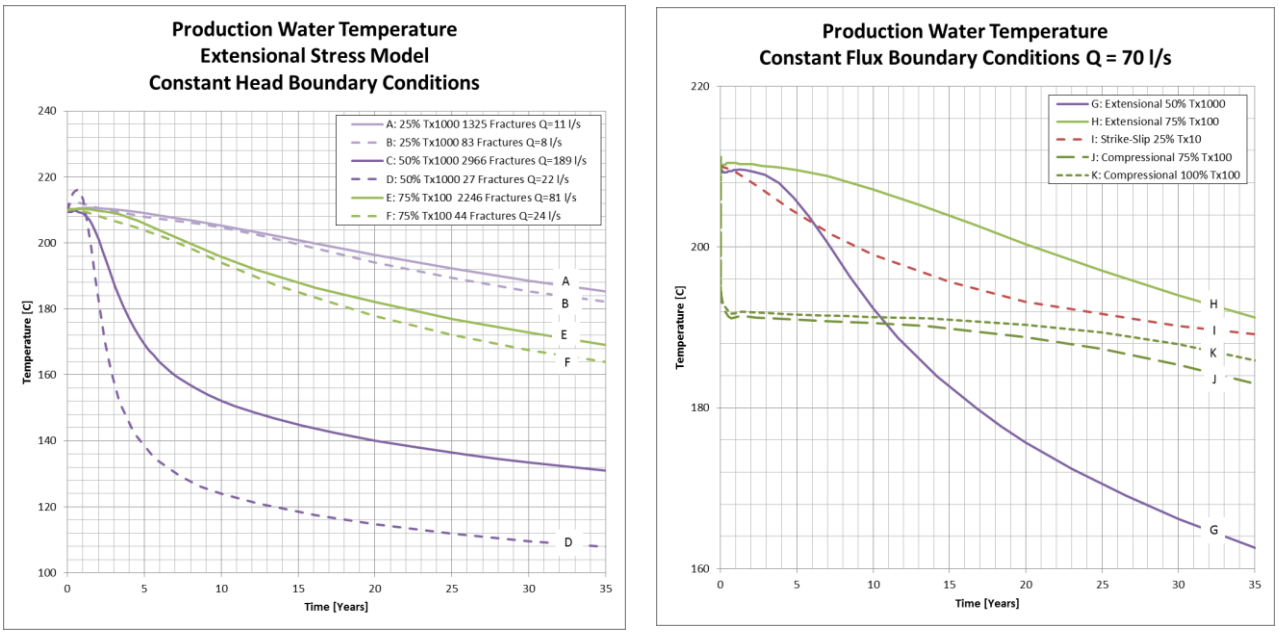

Figure 4. Production water temperature vs time for different models, stimulation levels and boundary conditions. Purple lines indicate critically stressed fracture transmissivities have been enhanced by a factor of 1000, green lines indicate a factor of 100 and red lines indicate a factor of 10. Percentages indicate what stimulation level was used. Labels A-G correspond to the matching simulations in Figures 2 and 3.

Figure 4b shows the thermal decline curves for the models requiring the lowest stimulation level and lowest transmissivity enhancement factor while meeting the low impedance criterion for the three stress states (see Figure 3). The compressional stress state model shows a rapid temperature drop to approximately 190°C. This is a consequence of the use of vertical wells. With vertical wells, the depth of the perforated section of the wells is 2950 m to 3550 m, connecting to significantly cooler water. As can be seen in Figure 5, the location of the fractures forming the connection between the two wells is at relatively shallow depths having temperatures in the 190°C range. While all three of the stress state models show potential for maintaining production water temperatures above 180°C for 20 years, the shape of the drawdown curves vary. The strike-slip model shows rapid thermal decline. The extensional model starts to decline after about 5 years, while the compressional stress model shows only limited thermal decline for 20 years. These differences can, in part, be understood by examining the model block geometries.

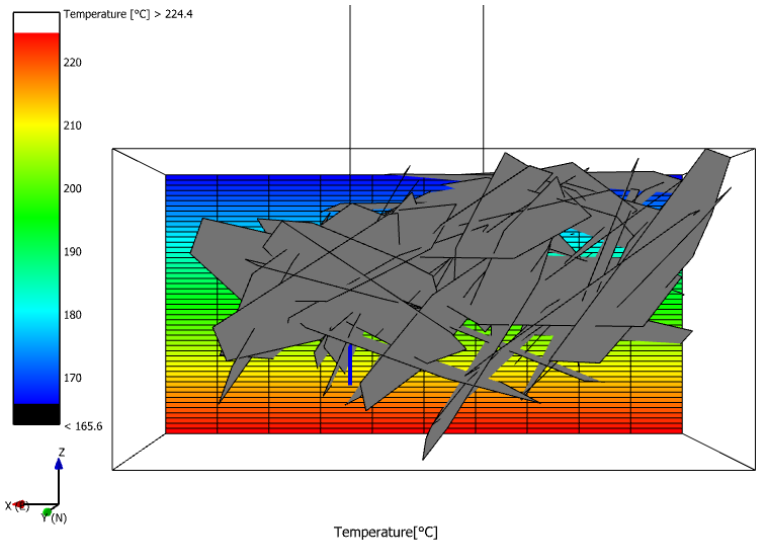

Figure 5. The temperature in the compressional stress model is shown along with the connected set of fractures forming the most conductive flow path in the model.

5. EVALUATING BLOCK SIZE AND SHAPE

For the purpose of this study, it is assumed that the blocks controlling EGS performance are defined by the "significantly" conducting fractures. These blocks are assumed to control the thermal evolution of the reservoir by defining the thermal diffusion distance (Warren and Root, 1963, Ranjbar and Hassanzadeh, 2011). Large blocks will take a relatively long time to conductively cool their interior, while smaller blocks release their heat much sooner in the reservoir lifetime. Block shape (e.g. box, slab and matchstick) also influences the rate of thermal depletion. Understanding these shapes at an EGS development site can help predict the selection site of successful well locations.

5.1 Defining Which Conducting Fractures Are Significant

The block size and shape definition above depends on how "significantly conducting" fractures is defined. The most transmissive fractures will accommodate most of the flow in a system but there may be different cut-off values depending upon if you are interested in the impedance of the system or if you want to understand the thermal drawdown history over a period of 20 years. The selection of the significant fracture sets may also depend on fracture orientation, spatial pattern and size which together control their connectivity. The rock thermal properties may also play a role with the range of potential thermal conductivity and heat capacity being in "competition" with the convective and conductive properties of the water within the smallest fractures.

Figure 6a illustrates the relationship between the impedance of the extensional stress state models vs the minimum transmissivity of the fractures included in the simulation. The transmissivity cut-off value based on the intersection of this best-fit line with the impedance value of 0.15 gives 8.4×10^{-6} m^2/s to use as a minimum transmissivity for defining block boundaries. Results from the strike-slip and compressional stress models show a lower minimum transmissivity line intercept, suggesting a model dependence of this value. However, for consistency the value of 8.4×10^{-6} m^2/s was assumed for all of the models.

Figure 6b shows another potential approach to selecting significant conducting fractures whereby the largest fractures in a model are selected based on different cut-off values of minimum transmissivity. The data displayed are for the extensional stress model using a transmissivity enhancement factor of 100. If more results were available, it might be possible to select the required minimum number of fractures or the minimum transmissivity value which capture most of the flow rate where the curve begins to level off.

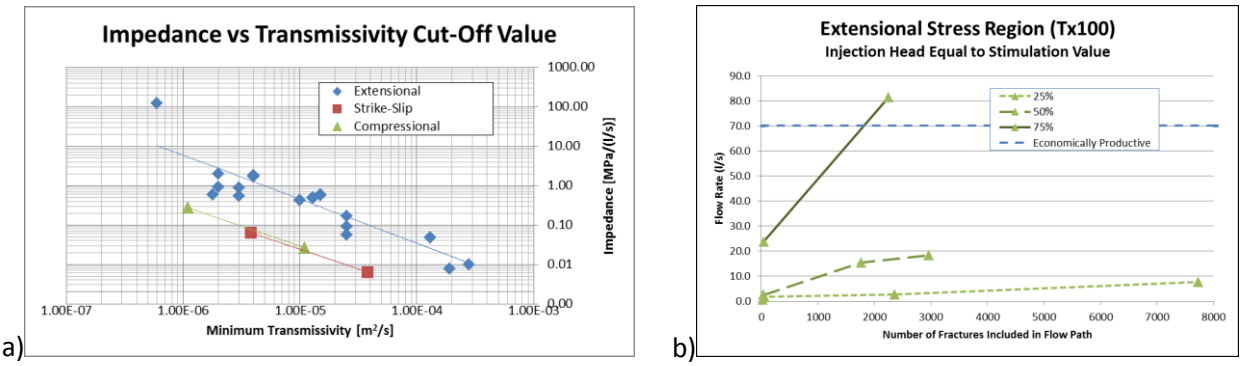

Figure 6. Methods for estimating minimum number of fractures needed to be included in a simulation. 6a shows impedance of models vs the transmissivity cut-off value used to select fractures for simulation. The values for the extensional stress model are used to estimate the minimum value used to define block boundaries. The plot on the right shows how flow rates vary with the number of fractures included in the simulation by stimulation level (only the largest and most transmissive fractures are used).

5.2 How Block Size Affects Thermal Drawdown

Block dimensions were calculated using the Multi-Dimensional Spacing algorithm (Golder Associates, 2015). For each randomly selected point in the DFN, a series of lines in user-specified directions are generated. The location of fractures intersected by each line is recorded. This leads to a spacing frequency distribution in several directions. Three orthogonal lines matching the orientations of the principal stress directions in each model were chosen. The spacing probability distributions are multiplied together using Monte Carlo sampling techniques to produce a frequency distribution of block volumes and surface areas. This is carried out by selecting X, Y and Z spacing values at random with selection probability proportional to their frequency, and multiplying them together to create a prismatic block. Each model used 1,000 sample points and generated 10,000 blocks for the analysis. Figure 7 shows an example of the block boundaries used to generate spacing frequency distributions for the strike-slip stress model as well as providing a schematic view of a reservoir block and the block size distribution in the σ_1 direction. The median block dimensions for all the DFN models at various stimulation levels are shown in Figure 8.

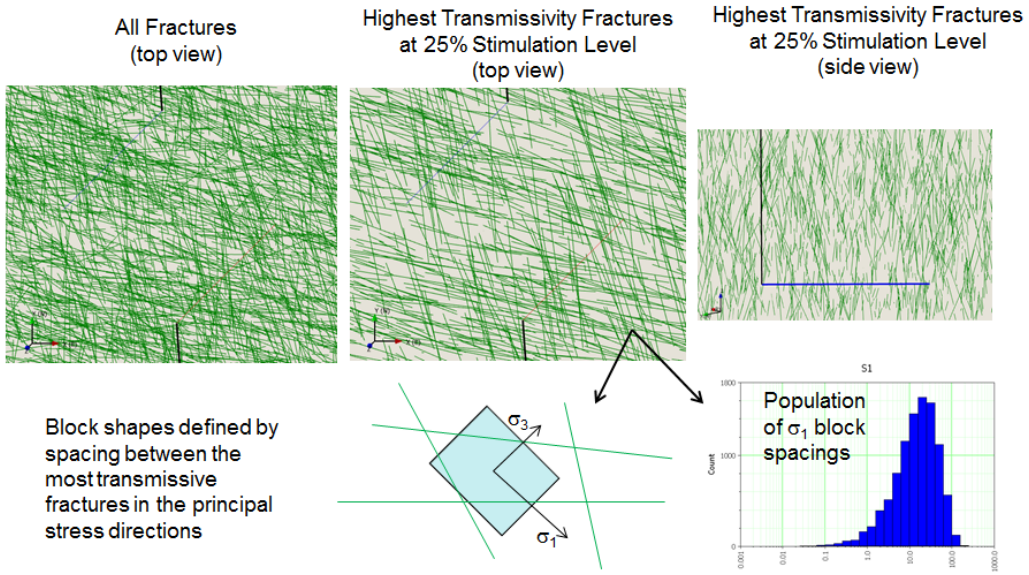

Figure 7. Top and side views of the strike-slip stress model after 25% level stimulation using a factor of 100 for the transmissivity enhancement to critically stressed fractures (2D slices showing fractures intersecting a plane surface). Block dimensions are collected in the principal stress directions. A representative population of blocks are generated using Monte Carlo sampling of these block dimensions.

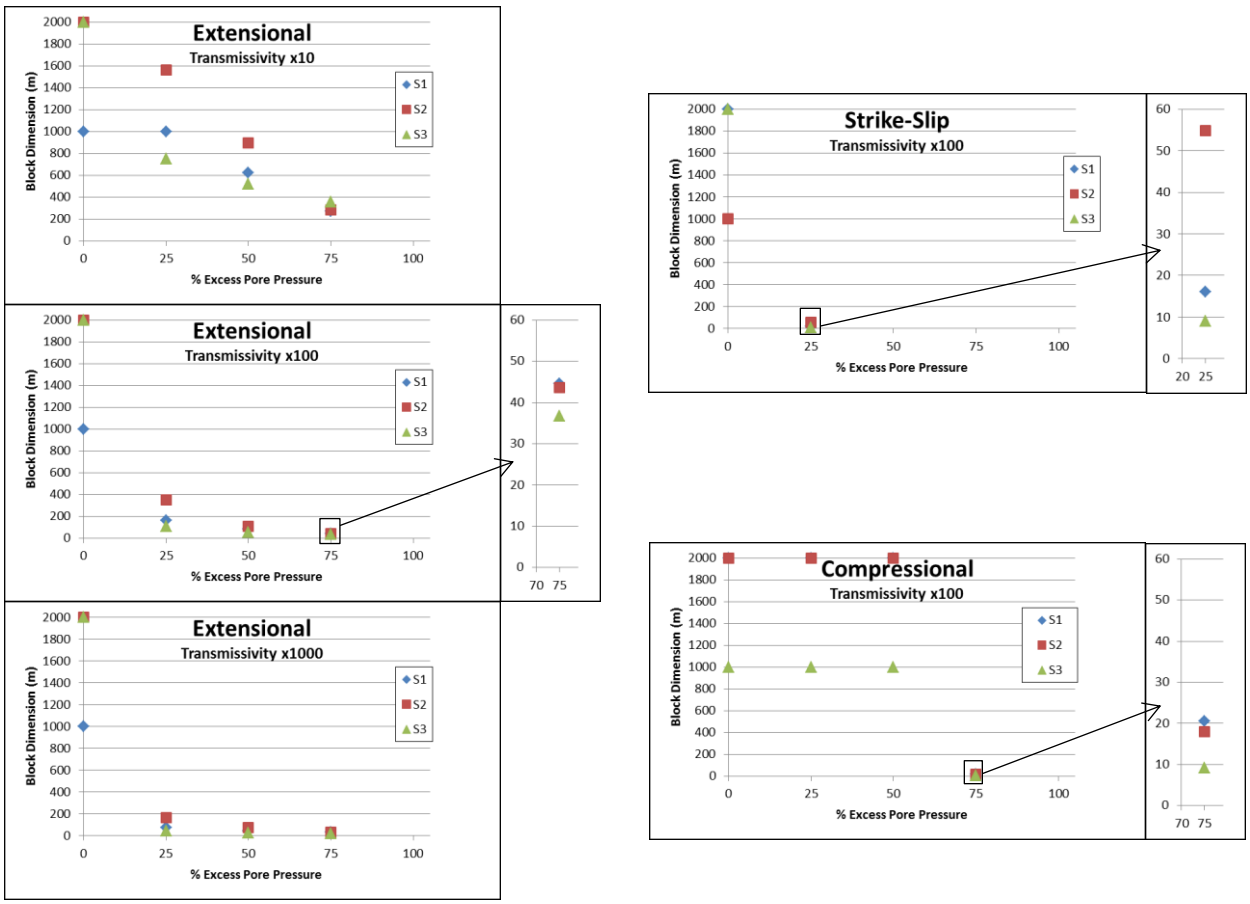

Figure 8. Median block dimensions in the principal stress directions σ_1, σ_2 and σ_3. Block boundaries are defined by fractures having transmissivity values above 8.4×10^{-6} m^2/s and the boundaries of the model. Detail views of the last stimulated level for some models shown on the right.

Figure 8 shows how the block shapes and sizes change with stimulation. Before stimulation, the block dimension is the model dimension, as no conductive fractures are included. As stimulation proceeds, the minimum block dimension is generally in the σ_3 direction as that is the average for critically stressed fractures. Figure 9 gives a schematic view of how the block size and shape are altered during stimulation.

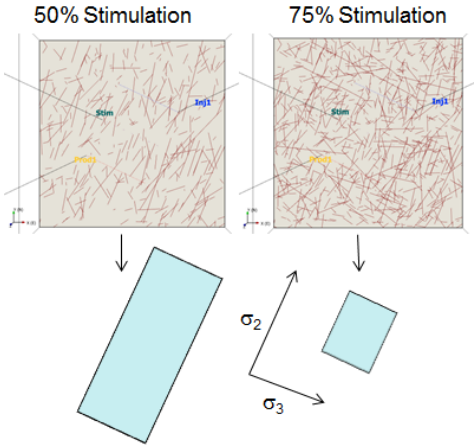

Figure 9. Top views of the extensional stress model after 50% and 75% stimulation level using a factor of 100 for the transmissivity enhancement to critically stressed fractures (2D slices showing fractures intersecting a plane surface at the well depth). Block size gets smaller and the shape changes from a more elongated rectangular prism to a more cubic shape. The minimum block size remains in the σ_3 direction.

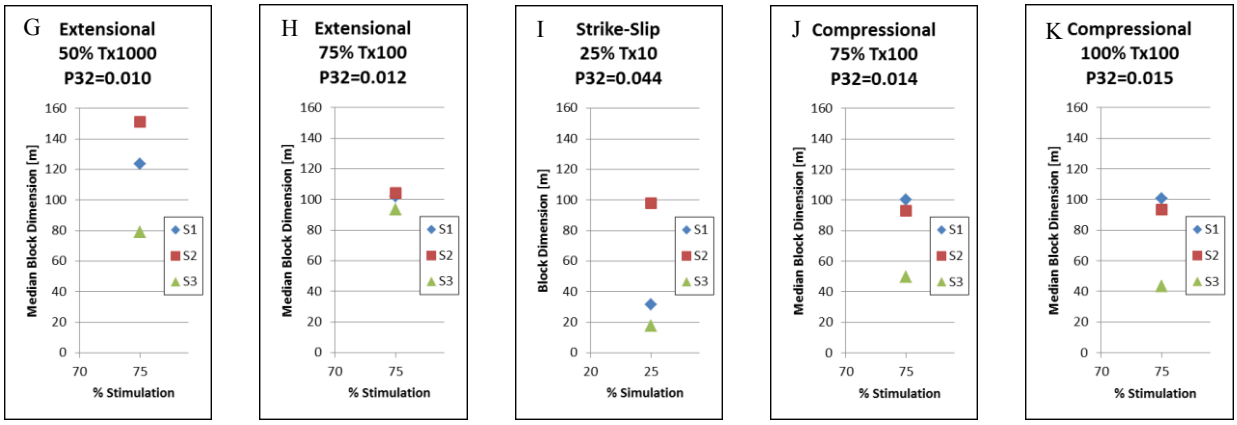

Figure 10. Median block dimensions in the principal stress directions for the five models that had their thermal declines simulated in Figure 4b. P_{32} is calculated as the total fracture area divided by the convex hull volume surrounding the fractures and is therefore a measure of how effectively the water is in contact with the reservoir rock. Labels G-K refer to the simulations shown in Figures 2-4.

The median block dimensions of the five models from Figure 4b are shown in Figure 10. While the absolute values are larger than the values reported in Figure 8 for the full DFN systems, reflecting the smaller numbers of fractures selected for the finite element modeling for thermal evolution, the relative lengths of the σ_1, σ_2 and σ_3 median values are almost identical. The minimum block dimensions correlate to the overall fracture intensity which is shown as volumetric fracture intensity P_{32} values for each model. Higher intensity (i.e. more fractures within a volume) results in smaller block sizes. Volumes for the simulations were calculated by fitting a convex polyhedron shape surrounding the fractures that were included in the simulation. These volumes ranged from 70% of the full reservoir volume for the compressional stress state model to close to 100% for both the extensional and strike-slip stress models. Generally, smaller block sizes in a system will result in a faster initiation of thermal decline as these small blocks cool quickly and stop contributing heat to the system, but this effect may be counteracted by having a larger overall fracture area in contact with the flowing water. The strike-slip stress model (I) has the smallest minimum block dimensions for both the σ_2 and σ_3 directions and also shows the most rapid initiation of thermal decline in Figure 4b as would be predicted based on block dimensions or fracture intensity alone. Using this same criterion, the compressional stress model should be the next fastest to show the initiation of thermal decline, however, that is not the case. The extensional model begins its thermal decline in 3-5 years while the compressional model only starts to show decline after 20 years. The fracture intensities are similar and, with its smaller stimulated volume and higher rock thermal conductivity, the

compressional stress system would be expected to chill out sooner. The anisotropy in the minimum block dimensions, with $\sigma_3 << \sigma_2 = \sigma_1$ shows that the fracture orientation is creating something of a layered system, similar to the parallel plate models of Gringarten (1975). Previous studies have shown that the parallel plate model systems perform better than systems having more complex fracture orientations (Doe et al., 2014) but another possible factor may be the thermal buffering available to this system that is not available to the extensional and compressional stress models as a result of the simulated fracture set inhabiting only a portion of the full model boundaries.

5.3 How Block Shape Affects Well Location

Understanding how natural fracture set orientations align with the expected orientations of critically stressed fractures after hydro-shearing allows for better siting of the injection/production wells relative to the stimulation well. In cases where the natural fractures align closely with the conjugate set first susceptible to Mohr-Coulomb failure (as in our strike-slip stress model (Figure 7)), the stimulated fractures should be well-connected and wells could be located to optimize flow path length. This also affects the positioning of horizontals wells. In cases where the natural fractures are not aligned with both conjugate sets (as in our extensional stress model), siting the wells so as to maximize the inter-well fracture connection may be a priority. Figure 11 shows how well locations can be selected to increase connectivity or flow path tortuosity (i.e. length). Fracture areas and surrounding rock volumes are an order of magnitude higher when wells are oriented in the σ_2 direction instead of the σ_3 direction.

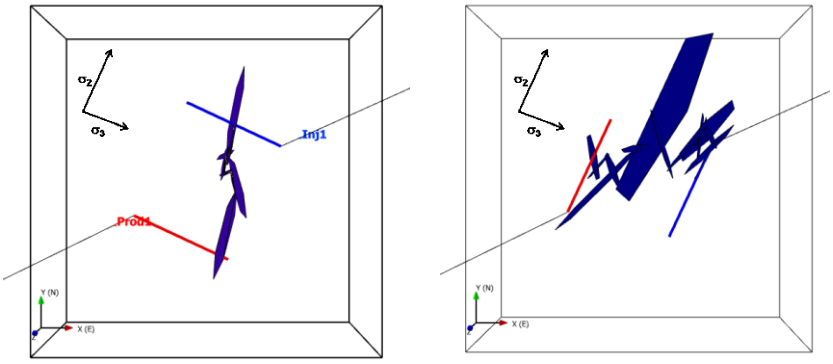

Figure 11. Top views of the extensional model showing the shortest fracture paths between wells having different geometries. DFN is from the extensional stress model at the 50% stimulation level using a transmissivity enhancement factor of 100.

CONCLUSIONS

When testing the feasibility of EGS systems, we must consider a broad range of conditions such as rock properties, fracture orientations, stress conditions and stimulation histories. Based on field study, assumptions may be made about how much fracture transmissivity is enhanced by stimulation. To achieve computational efficiency, fracture populations must somehow be simplified yet retain those properties that govern the behavior of the system with respect to EGS performance. Through the use of the models and techniques outlined here, which are based on geologically reasonable parameters and complexity, one can examine the changing behavior of EGS systems as they undergo hydraulic stimulation. This allows us to gauge the importance of certain parameters and may bring common patterns to light.

Knowing the stress state and orientation of the natural fractures is key to knowing how much stimulation pumping pressure is expected to be necessary to get a system that can support economic flow rates. Our strike-slip stress model, having natural fracture sets aligning closely with the earliest slipping orientations is relatively easily stimulated. Our compressional stress model experiences much higher stress conditions and did not have natural fracture sets closely aligned with those first to fail in shear and required a much higher stimulation level in order to reach an economic flow rate. The extensional stress model fell somewhere in between, but showed significant block shape changes as stimulation levels increased, due to the partial alignment with the initial critically stressed fractures.

When actual fracture aperture widths within individual fractures are calculated during simulation, as was done in our induced hydraulic fractures for the extensional stress model at 100% stimulation level, the apertures in vertical fractures tend to increase at shallower depths due to the stress gradient differentials. This was not a large effect in the induced hydraulic fractures in the compressional stress model due to their horizontal orientation where the local stress conditions remained constant throughout the fracture. While the majority of the simulations in this paper were performed on fractures having a constant aperture, with adjustments for enhanced transmissivity as a result of having their center positions being critically stressed, it is likely that this simplification leads to an overestimation of the flow rates in deeper portions of the fracture.

The strike-slip stress model was effectively stimulated, defined as having an impedance below 0.15 MPa/(l/s), using any of the three fracture transmissivity enhancement factors considered in the paper (10, 100, 1000). The extensional stress model and the compressional stress model required transmissivity factors of 100 or 1000. Clearly this result is dependent upon the original transmissivities in each model. Highlighted by this paper is the dependency on the alignment between the natural fracture set orientations and the stress state. If the natural fractures are not aligned, then a higher stimulation level or a larger transmissivity enhancement factor may be required.

Examination of block shape and size in the stimulated reservoir show that minimum block dimensions always align with the minimum principal stress direction as stimulation proceeds, at least relative to the other principal stress directions. The relative sizes of the other two block dimensions control the basic block shape, whether cubic, columnar or planar. This block shape and orientation control the flow path geometry where planar blocks force flow paths in particular directions, an anisotropy that can be exploited in choosing well locations.

ACKNOWLEDGMENTS

The authors gratefully acknowledge the funding support of Sandia Laboratories and the US Department of Energy.

REFERENCES

Breede, K., Dzebisashvili, K., Liu, X., and Falcone, G.: A Systematic Review of Enhanced (or Engineered) Geothermal Systems: Past, Present and Future, *Geothermal Energy*, **1**:4, (2013), 1-27.

Brunner, P., and Simmons, C.: HydroGeoSphere: A Fully Integrated, Physically Based Hydrological Model, *Ground Water*, **50** (2012), 170-176.

Dempsey, D., Kelkar, S., Davatzes, N, Hickman, S., Moos, D., and Zemach, E.: Evaluating the roles of Thermoelastic and Poroelastic Stress Changes in the Desert Peak EGS Stimulation, *Proceedings, Thirty-Ninth Workshop on Geothermal Reservoir Engineering*, Stanford University, February 24-26, (2014), 1-14.

Doe, T., McLaren, R., and Dershowitz, W.: Discrete Fracture Network Simulations of Enhanced Geothermal Systems, *Proceedings, Thirty-Ninth Workshop on Geothermal Reservoir Engineering*, Stanford University, February 24-26, (2014), 1-11.

Finnila, A., Dershowitz, W., Doe, T., and McLaren, R.: Hydro-shearing and Hydraulic Fracturing for Enhanced Geothermal Systems in Archetypical Normal, Strike-Slip and Thrust Faulting Terrains, *GRC Transactions*, **39**, (2015), 1-19.

Golder Associates: FracMan7 Interactive Discrete Feature Data Analysis, Geometric Modeling and Exploration Simulation, User Documentation, v.7.51, (2015), 1-525.

Idaho National Laboratory: The Future of Geothermal Energy Impact of Enhanced Geothermal Systems (EGS) on the United States in the 21st Century, INL/EXT-06-11746, (2006), 1-372.

JASON: Enhanced Geothermal Systems, JSR-13-320, MITRE Corporation, McLean, VA, (2013), 1-141.

Miller, I., Lee, G., and Dershowitz, W.: MAFIC Matrix/Fracture Interaction Flow and Transport Code. User Documentation, Version 1.72., Golder Associates, Inc., Seattle, (2005).

Miller, S.A.: Modeling Enhanced Geothermal Systems and the Essential Nature of Large-Scale Changes in Permeability at the Onset of Slip, *Geofluids*, **15**, (2015), 338-349.

Ranjbar, E., and Hassanzadeh, H.: Matrix-Fracture Transfer Shape Factor for Modeling Flow of a Compressible Fluid in Dual-Porosity Media, *Adv. Water Res.,* **34**, (2011), 627-639.

Therrien, R., and Sudicky, E.A.: Three-Dimensional Analysis of Variably-Saturated Flow and Solute Transport in Discretely-Fractured Porous Media, *Journal of Cont. Hyd.*, **23**(1-2), (1996), 1-44.

Warren, J. E., and Root, P. J.: The Behavior of Naturally Fractured Reservoirs, *Soc. Pet. Eng. J.*, (1963), 245-255.